VOL. 54
NO. 1
JANUARY
2021

JCEJ

JOURNAL OF CHEMICAL ENGINEERING OF JAPAN

[VOL. 54, NO. 1, JANUARY 2021]

SCEJ The Society of Chemical Engineers, Japan

The Society of Chemical Engineers, Japan

JCEJAQ 54(1)
1-50(2021)
ISSN 0021-9592

Journal of Chemical Engineering of Japan, Vol. 54, No. 1, pp. 1–11, 2021 **Research Paper**

Reaction Engineering Approach to Turbulence Modelling —Universal Law of the Wall, Pipe Flow, and Planar Jet Flow

Xiao Dong Chen and Siyu Zou

School of Chemical and Environmental Engineering, Soochow University, Suzhou Industrial Park Campus, Jiangsu Province, China

Keywords: Reaction Engineering Approach, Universal Law of the Wall (ULW), Near Wall Velocity Distribution, Reynolds Stress, Flow in Circular Pipe, Flow in Turbulent Planar Jet

Although engineering turbulence modeling is a well-established field, there is room for new ideas. In the current work, the rate of Reynolds stress generation is considered the product of a probability coefficient dependent on the viscous effect over the inertia effect and an energetic parameter expressed in terms of velocity dependence. The rate of Reynolds stress dissipation is defined as a simple second-order power function; this function emphasizes the nature of the local interactions (molecular level at their origins) that are similar to those for the reaction. Hence, the current approach can be called a reaction engineering approach for turbulence. Examples analyzed with this approach are: 1) the Universal Law of the Wall; 2) diameter-wide axial velocity distribution of the circular pipe (internal flow); 3) bulk behavior of the axial velocity distribution for a turbulent planar jet (external flow); and 4) far-field axial velocity distribution for a planar jet with numerical simulations. These findings suggest the potential of this approach for future exploration.

Introduction

Turbulence modelling still fascinates many engineering researchers. For engineering applications with complex geometries and over vast spaces often makes cost-effective computation desirable. Before the emergence of direct numerical simulation (DNS), engineering models with intuitive assumptions were used to yield useful solutions to complex industrial problems; time-averaged Reynolds stresses were resolved. Several "universal" empirical coefficients were used for these models. However, only a handful of models such as the k–ε models were successful and widely applied in engineering practices. The DNS approach requires large computational power when a realistic dimension is considered; further, bifurcation and initial value scenarios may affect its computational end-points, which are aspects that are yet to be fully understood. Thus, DNS has mainly been employed to reveal flow structures including investigating the transition from laminar to turbulent flows in small or narrow domains (Hof *et al.*, 2010; Avila *et al.*, 2011; Barkley *et al.*, 2015; Kühnen *et al.*, 2018).

The Boussinesq assumption, which assumes that the Reynolds stress is proportional to the mean time-averaged velocity gradients is generally considered for engineering (White, 1974; Chen, 1984; Hrenya *et al.*, 1995; Bird *et al.*, 2002; Schlichting and Gersten, 2003; Thornber *et al.*, 2007; Eskin, 2017).

However, in this study, a different approach is considered. Firstly, a mathematical expression describing local turbulence is proposed, followed by the analytical work of well-known scenarios such as the universal law of the wall (ULW), circular pipe flow, and turbulent planar jet. Finally, a numerical simulation of the planar jet was conducted, which employed the simplified model.

Received on March 27, 2020; accepted on November 4, 2020
DOI: 10.1252/jcej.20we056
Correspondence concerning this article should be addressed to X. D. Chen (E-mail address: xdchen@mail.suda.edu.cn).

1. Main Derivations, Results, and Discussion

1.1 Universal Law of the Wall

Laufer (1952) and Churchill (1997, 2000) started their boundary layer analyses from flow phenomena in a pipe. In these notable works, the momentum equation (Navier–Stokes equation) for time-averaged behavior in fully developed turbulence in a smooth circular pipe was commonly equated as

$$\overline{u'v'} = \nu\frac{\partial \bar{u}}{\partial r} + \frac{r}{R}u_r^2 \tag{1}$$

The LHS is a Reynolds stress, and u_r denotes the friction velocity [m·s^{-1}]. In terms of the distance from the wall surface y, instead of r, one can write

$$\overline{u'v'} = \upsilon\frac{\partial \bar{u}}{\partial (R-y)} + \left(\frac{R-y}{R}\right)u_r^2 = -\upsilon\frac{\partial \bar{u}}{\partial y} + \left(1-\frac{y}{R}\right)u_r^2 \tag{2}$$

where $y = R - r$ (> 0) (see **Figure 1**); R denotes the radius of the pipe [m]; u' and v' denote the fluctuating velocity components in the x and y directions, respectively [m·s^{-1}]; υ represents the kinematic viscosity [m^2·s^{-1}] equal to μ/ρ; μ denotes the fluid viscosity [Pa·s]; and ρ represents the density of the fluid [kg·m^{-3}].

The friction velocity u_r is defined as a function of the wall shear stress $\bar{\tau}_w$ and the fluid density ρ as

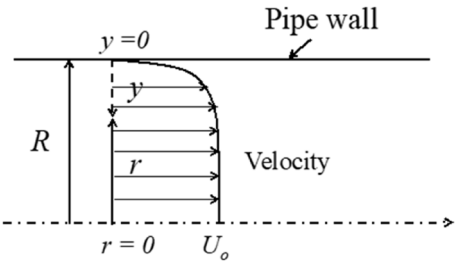

Fig. 1 Schematic of the turbulent flow velocity profile in a pipe and related coordinate system used

$$u_r = \sqrt{\frac{\overline{\tau}_w}{\rho}} \tag{3}$$

The dimensionless velocity and dimensionless distance from the wall, respectively, u^+ and y^+, are defined as

$$u^+ = \frac{\overline{u}}{u_r} \tag{4}$$

$$y^+ = \frac{y}{\delta_v} \tag{5}$$

where δ_v denotes the wall layer thickness (referred to as the flow length scale); it is given by

$$\delta_v = \frac{\upsilon}{u_r} \tag{6}$$

In the near-wall region, the dimensionless velocity u^+ against the dimensionless distance from the wall y^+ is known to exhibit a unique single relationship. The relationship is called the Universal Law of the Wall (ULW). In the past, many researchers have attempted to construct a single equation to describe the ULW; for example, those expressed by Flint (1967) and Patel (1973). Flint's equation, $u^+(y^+)$ for $y^+ = 0$–100, works well against experimental data:

$$u^+ = 2.5\ln(1+\kappa y^+) + C_1\left[1-\exp\left(-\frac{y^+}{11}\right)-\frac{y^+}{11}\exp(-0.33y^+)\right] \tag{7a}$$

where $\kappa = 0.4$ and $C_1 = 7.3$; 11 represents the value for y^+ at which the generation of turbulence was the highest (Laufer, 1952). This formula is not explicit in conforming to $u^+ = y^+$ for $y^+ < 5$. Another good example is the correlation by Spalding (1961) that expresses y^+ as a function of u^+; this fits well with the available experimental data points provided by Sherwood *et al.* (1968).

$$y^+ = u^+ + 5.32\times10^{-2}(u^+)^2 - 7.68\times10^{-3}(u^+)^3 + 2.19\times10^{-4}(u^+)^4 + 1.64\times10^{-4}(u^+)^5 - 2.16\times10^{-5}(u^+)^6 + 9.12\times10^{-7}(u^+)^7 \tag{7b}$$

For the near-wall scenario ($r\to R$ or $y\to 0$) in the current approach, Eq. (2) can be simplified to

$$\overline{u'v'} \approx -\upsilon\frac{\partial\overline{u}}{\partial y} + u_r^2 \tag{8}$$

Here, the local Reynolds stress in the boundary layer domain is considered to be consumed and transported once it is generated as given by

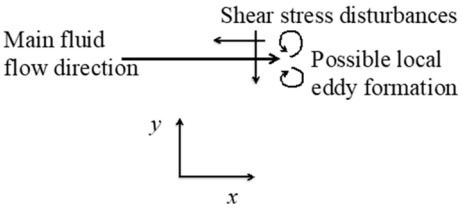

Fig. 2 Two-dimensional illustration of the intuitive mechanism for triggering local eddies leading to turbulence

$$\frac{\partial\overline{u'v'}}{\partial t} + \overline{v}\frac{\partial\overline{u'v'}}{\partial y} \approx \upsilon\frac{\partial^2\overline{u'v'}}{\partial y^2} + \dot{G} - \dot{D} \tag{9}$$

This expression is in planar coordinates (x and y); υ denotes a type of diffusivity for the diffusive transport of turbulent stress in conventional wisdom. Equation (9) "controls" the Reynold stress. The generation and dissipation of local turbulence is considered a result of local fluid (molecules) interactions at the same spot (a stirrer spins interacting with the fluid). As soon as turbulent energy is created, it starts to dissipate simultaneously at the same spot because of its viscous nature; for simplicity, the pressure–shear correlation effect is not considered. Equation (9) is not the same as that described conventionally (Schlichting and Gersten, 2003).

If one considers generation and dissipation as types of molecular interaction, similar to that for a chemical reaction, they may not be considered as functions of velocity gradients and may be expressed as mathematical functions reflecting the interactive nature of the phenomena. Hence, a chemical conservation-like expression can be stipulated as

$$\frac{\partial\overline{u'v'}}{\partial t} + \overline{v}\frac{\partial\overline{u'v'}}{\partial y} \approx \upsilon\frac{\partial^2\overline{u'v'}}{\partial y^2} + f_1(\gamma,\overline{u}) - f_2\left(\overline{u'v'}\right) \tag{10}$$

There are two source terms in the above equation that are not conventional. f_1 represents the local rate of turbulence generation that is a function of the local equivalence of the Reynolds number γ and the time-averaged local velocity $\bar{u}$. Increasing the Reynolds number over a critical limit will lead to a commonly recognized turbulent state, and the formation of an eddy (a type of local fluid rolling behavior)—essential for turbulence—is easier if the inertia is not as strong as that compared with the shearing effect (viscous effect) to allow the fluid to "make a turn" (**Figure 2**). As such, the overall developing turbulence that is dependent on the Reynolds number appears to be a "net effect" generated by the combination of the tendency to roll or to form an eddy, and it is positively related to $1/\gamma$ rather than γ and the increase in fluid velocity. The increase in velocity, and hence the increase in the power of the fluid motion can caused the eddy formation to be more rigorous, violent, and sustainable. Further, the tendency to roll or to form eddy alone is insufficient to lead to an energetic state required for observing turbulence phenomena. Therefore, f_1 is aimed at reflecting the physics described above, and f_2 represents the rate of

turbulence dissipation that reflects the fact that greater the local turbulence, the greater is the local dissipation. Indeed, as soon as turbulence starts, its dissipation commences.

As described by Chen (2019), parameter γ is the local equivalence of the Reynolds number (Chen, 2019) (and it is not a local Reynolds number); it represents the ratio of the effect of inertia and the effect of viscous force at the same location/spot and is given by

$$\gamma = \frac{\rho \overline{u}^2}{\mu \left| \frac{\partial \overline{u}}{\partial y} \right|} \tag{11}$$

In an usual two-dimensional fluid flow scenario, shear stresses in both directions (x and y) affect the process. Only the parallel layer is considered as the boundary layer in this study. The characteristics of how the local derivative of γ (defined in Eq. (11)) changes with increasing velocity determines the onset of turbulence. The effect in one direction (y) is the most important; effects of the parameters in different directions must be considered when the boundary layer assumption is no longer valid (refer to Figure 2 for the general two-dimensional case). Tao *et al.* (2013) proposed a local Reynolds number to represent the maximum ratio of the energy supply to and the energy dissipation within a cross-section of a channel. This local Reynolds number at its largest was found to be similar at the transition thresholds of laminar to turbulence flow for three basic internal flow scenarios. Most recently, Pavlíček (2019), following the ideas of Tao *et al.* (2013) and Chen (2019) proposed calculating the local Reynolds number by numerically adding the inertia terms and dividing it by the summation of all viscous stress terms. All studies recognize that the local ratio of inertia to viscous stress is one of the most important indicators of the fluid condition.

Based on the intuition of Chen (2019), a certain combination of γ and velocity that can qualify the intensity of turbulence is suggested.

The nature of interactions in the fluid are like molecular interactions, and therefore, mechanisms instituted in Eq. (10) can be represented using power laws (rate expressions like those in chemical reaction engineering) (Levenspiel, 1999). This approach can be called the reaction engineering approach (REA).

According to chemical reaction engineering, interactive power functions are used to formulate f_1 and f_2 as

$$f_1 = k_g \left(\frac{1}{\gamma} \right)^m (\overline{u}^2)^n \tag{12}$$

$$f_2 = k_d \left(\overline{u'v'} \right)^p \tag{13}$$

where k_g and k_d are positive rate constants for turbulence generation and dissipation, respectively; their units vary depending on the choices of n and p, respectively.

Equation (10) can be rewritten as

$$\frac{\partial \overline{u'v'}}{\partial t} + \overline{v} \frac{\partial \overline{u'v'}}{\partial y} = \upsilon \frac{\partial^2 \overline{u'v'}}{\partial y^2} + k_g \left(\frac{1}{\gamma} \right)^m (\overline{u}^2)^n - k_d \left(\overline{u'v'} \right)^p \tag{14}$$

Explicitly, Eq. (14) becomes

$$\frac{\partial \overline{u'v'}}{\partial t} + \overline{v} \frac{\partial \overline{u'v'}}{\partial y} = \upsilon \frac{\partial^2 \overline{u'v'}}{\partial y^2} + k_g \left[\upsilon \frac{\partial \overline{u}/\partial y}{\overline{u}^2} \right]^m (\overline{u}^2)^n - k_d \left(\overline{u'v'} \right)^p \tag{15}$$

To obtain an analytical expression considering the pseudo-steady state and neglecting the effect of diffusive and convection transport in the y-direction for simplicity, the above conservation equation is reduced to

$$k_g \left[\upsilon \frac{\partial \overline{u}/\partial y}{\overline{u}^2} \right]^m (\overline{u}^2)^n = k_d \left(\overline{u'v'} \right)^p \tag{16}$$

A simple relationship between the Reynolds stress and the velocity can be found as

$$\overline{u'v'} = \left(\frac{k_g}{k_d} \right)^{\frac{1}{p}} \left(\upsilon \frac{\partial \overline{u}}{\partial y} \right)^{\frac{m}{p}} (\overline{u}^2)^{\frac{n-m}{p}} \tag{17}$$

where p is considered is set as 2 as suggested in Appendix 1.

A good starting point is to consider $m = 2$ for simplicity.

Note that the $1/j$-th law approximates the time-averaged turbulent velocity profile in pipe flow or plate flow well (Bird *et al*, 2002; Chen, 2019). The most well-known law is $j = 7$. Therefore, as a first approximation, $n = 8$ is considered. The above equation can be rewritten as

$$\overline{u'v'} = \upsilon \left(\frac{k_g}{k_d} \right)^{\frac{1}{2}} \overline{u}^6 \frac{\partial \overline{u}}{\partial y} > 0 \tag{18}$$

The above equation emphasizes that turbulence generation increases rapidly in intensity as velocity increases. Therefore, substituting the Reynolds stress in Eq. (8) with Eq. (18) leads to

$$\upsilon \left(\frac{k_g}{k_d} \right)^{\frac{1}{2}} \overline{u}^6 \frac{\partial \overline{u}}{\partial y} + \upsilon \frac{\partial \overline{u}}{\partial y} - u_r^2 = 0 \tag{19}$$

Normalizing Eq. (19) according to Eqs. (4) and (5),

$$\left[\frac{1}{7} \left(\frac{k_g}{k_d} \right)^{\frac{1}{2}} u_r^6 \right] \frac{\partial (u^+)^7}{\partial y^+} + \frac{\partial u^+}{\partial y^+} - 1 = 0 \tag{20}$$

Grouping the coefficients associated with the first term of the LHS of Eq. (20) to be represented as α,

$$\alpha \frac{\partial (u^+)^7}{\partial y^+} + \frac{\partial u^+}{\partial y^+} - 1 = 0 \tag{21}$$

By simply integrating Eq. (21) from $y^+ = 0$, $u^+ = 0$ to $y^+ > 0$, $u^+ > 0$, we obtain

$$\alpha (u^+)^7 + u^+ - y^+ = 0 \tag{22}$$

Equation (22) naturally satisfies the wall requirement

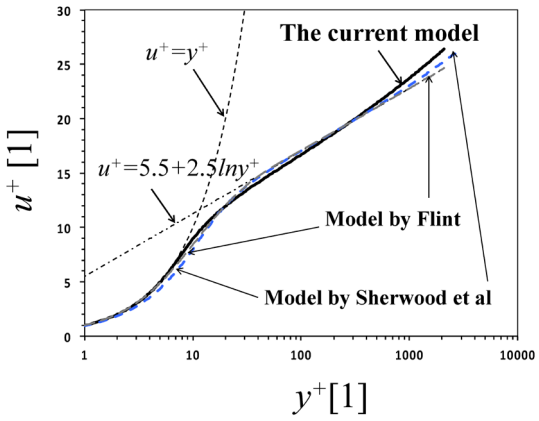

Fig. 3 Comparison among the good models of the ULW plots and the current model (Note: The model by Flint becomes similar to the log-law at high y^+)

for $y^+ \to 0$. Further, as y^+ increases, the $(u^+)^7$ term becomes dominant. To obtain the coefficient and considering one set of values from the ULW plot from the model by Flint (1967) or the log-law, i.e., $y^+ = 267.0$ and $u^+ = 19.5$, one finds

$$a \approx 2.31 \times 10^{-7}$$

For a large y^+, this approaches the well known1/7-th law given as

$$u^+ \approx 8.87(y^+)^{\frac{1}{7}} \tag{23}$$

Figure 3 illustrates how good such a simple relationship (Eq. (22)) works out.

To generalize the approach, one should not be limited to the simple format for f_2 in Eq. (10) because the 1/7-th law is an approximation. Further,

$$f_4(u^+) + u^+ - y^+ = 0$$

or

$$y^+ = u^+ + f_4(u^+) \tag{24}$$

describes the ULW in the most accurate way possible. Eq. (24) is in good contrast to the early models, and the famous log-law for the wall turbulence proposed by von Karman was actually empirical (Churchill, 1997).

1.2 Pipe flow

Based on the above analysis on the near-wall region, the LHS with Eq. (1) was substituted with Eq. (18) to understand the pipe-wide approach for fully developed turbulent flow.

$$\upsilon\left(\frac{k_g}{k_d}\right)^{\frac{1}{2}} \overline{u}^6 \frac{\partial \overline{u}}{\partial y} = -\upsilon \frac{\partial \overline{u}}{\partial y} + \left(1 - \frac{y}{R}\right) u_r^2 \tag{25}$$

For simplicity, a pseudo-steady state was assumed for Reynolds stress. Nevertheless, one can further rewrite Eq. (25) as

$$\left[1 + \left(\frac{k_g}{k_d}\right)^{\frac{1}{2}} \overline{u}^6\right] \frac{\partial \overline{u}}{\partial \eta} - \left(\frac{u_r^2 R}{\upsilon}\right)(1-\eta) = 0 \tag{26}$$

where $\eta = y/R = 1 - r/R$; r denotes the radial coordinate, and R denotes the inner radius of the pipe of concern. When $r = 0$, $\eta = 1$, Eq. (26) ensures that the velocity gradient is zero. Integrating from $\eta = 0$ to any $\eta \leq 1$ and rearranging the terms yields

$$\left(\frac{\overline{u}}{U_o}\right) + \alpha\left(\frac{u_r}{U_o}\right)^{-6}\left(\frac{\overline{u}}{U_o}\right)^7 - \left(\frac{u_r}{U_o}\right)\left(\frac{R}{\delta_v}\right)\left(\eta - \frac{1}{2}\eta^2\right) = 0 \tag{27}$$

where U_o denotes the maximum velocity at $\eta = 1$. Assuming a coefficient α of 1, the following equation can be obtained.

$$\left(\frac{\overline{u}}{U_o}\right) + \alpha_1\left(\frac{\overline{u}}{U_o}\right)^7 - \beta\left(\eta - \frac{1}{2}\eta^2\right) = 0 \tag{28}$$

or

$$\left(\frac{\overline{u}}{U_o}\right)^7 + \frac{1}{\alpha_1}\left(\frac{\overline{u}}{U_o}\right) - \frac{\beta}{\alpha_1}\eta + \frac{\beta}{2\alpha_1}\eta^2 = 0 \tag{29}$$

For $r = 0$ and $\eta = 1$,

$$\beta = 2(\alpha_1 + 1), \quad \alpha_1 = \alpha\left(\frac{u_r}{U_o}\right)^{-6} \tag{30}$$

Finally,

$$\left(\frac{\overline{u}}{U_o}\right)^7 + \frac{1}{\alpha_1}\left(\frac{\overline{u}}{U_o}\right) - 2\left(1 + \frac{1}{\alpha_1}\right)\eta + \left(1 + \frac{1}{\alpha_1}\right)\eta^2 = 0 \tag{31}$$

This is a new result; further, this can be rearranged to

$$\eta^2 - 2\eta + \left[\frac{\alpha_1}{\alpha_1 + 1}\left(\frac{\overline{u}}{U_o}\right)^7 + \frac{1}{\alpha_1 + 1}\left(\frac{\overline{u}}{U_o}\right)\right] = 0 \tag{32}$$

which leads to

$$\eta = 1 - \sqrt{1 - \left[\frac{\alpha_1}{\alpha_1 + 1}\left(\frac{\overline{u}}{U_o}\right)^7 + \frac{1}{\alpha_1 + 1}\left(\frac{\overline{u}}{U_o}\right)\right]} \tag{33}$$

which can be written in r/R as

$$\frac{\alpha_1}{\alpha_1 + 1}\left(\frac{\overline{u}}{U_o}\right)^7 + \frac{1}{\alpha_1 + 1}\left(\frac{\overline{u}}{U_o}\right) = 1 - \left(\frac{r}{R}\right)^2 \tag{34}$$

The RHS of the above equation is the well-known parabolic velocity profile for a fully developed laminar flow in a circular pipe.

Because the value of α is known approximately from the ULW analysis—2.31×10^{-7}—with the case for fully developed turbulence in the pipe and for $Re_o = 1{,}620 \times 10^3$ (based on pipe radius) or for $Re = 3{,}240 \times 10^3$ (based on the pipe diameter) as reported in Pai (1953), $u_r/U_o = 0.0253$, and $\alpha_1 \approx 880.26$.

The velocity ratio u_r/U_o is determined based on the relationship with the friction factor. For a pipe, the velocity ratio u_r/U_o can be obtained from the friction factor (Λ) correlation (White, 1974) for the turbulent regime as

$$\Lambda = 0.495\,(\log Re)^{-2.2} \tag{35}$$

which is within ±2% of the historical data. The *Re* here is defined as

$$Re = \frac{\rho u_{\text{ave}}(2R)}{\mu} \tag{36}$$

where u_{ave} denotes the mean velocity.

The relationship between the friction factor and velocity is given as

$$\Lambda = 8\left(\frac{u_r}{u_{\text{ave}}}\right)^2 \tag{37}$$

The average velocity $u_{\text{ave}} = 4/5U_o$.

The friction velocity ratio can be obtained for different *Re* (based on diameter) in the turbulence regime. With these valuable parameters, one obtains the velocity profile for a fully developed turbulent flow in a circular pipe based on Eq. (33). The velocity profile for the fully developed turbulence in a circular pipe is described using the $1/q$-th law (Eq. (38)), which is well known to account for greatest portion of the profile (Cengel and Cimbala, 2014). The value of q increases with increasing Reynolds number, such as 7, 8, or 10 (Kudela, 2014). The value $q = 7$ is most often quoted in engineering textbooks.

$$\frac{\overline{u}}{U_o} = \left(1 - \frac{r}{R}\right)^{1/q} \tag{38}$$

The above power–law profile cannot be used to calculate wall shear stress because it yields a velocity gradient of infinity (at $r = R$). Further, it fails to obtain zero slope at $r = 0$. For $Re_o = 1{,}620\times10^3$, q can be obtained based on its relationship with *Re* as approximately 9.5 (Kudela, 2014) . A comparison between the $q = 9.5$ case with the current model calculation is shown in **Figure 4**. The current model can satisfy both the wall condition (i.e., ULW) and the center condition (at $r = 0$, the velocity gradient is zero).

Perhaps the most important comparison to support the current model is the one with the model proposed by Pai (1953); this is because Pai's model was benchmarked well with the famous Nikuradse dataset on pipe flow at the same *Re* ($3{,}240\times10^3$; see Figure 4).

$$\frac{\overline{u}}{U_o} = 1 - a\left(\frac{r}{R}\right)^2 - (1-a)\left(\frac{r}{R}\right)^{32} \tag{39}$$

For pipe flow, $a = 0.204$ (Pai, 1953). Further, Pai's formula was successful in matching the experimental results of Laufer (1950) for rectangular channel flow at $Re = 12{,}300$, except in this case, a different value of 0.33 was found suitable (White, 1974).

The Pai model does not conform to the ULW. Changing the Reynolds number in the turbulent regime for a pipe does not affect the conclusion for the current model. When *Re* becomes small, like a few hundreds, Eq. (34) is reduced naturally to the laminar parabolic profile as α_1 can become considerably smaller than 1.

1.3 Planar jet

1.3.1 Approximate calculations Turbulent planar jet flow is an interesting phenomenon and a well-resolved problem (**Figure 5**); hence, it is excellent for demonstrating the current approach. According to the turbulent planar jet theory, for a sufficiently far downstream—the far field from the jet entry or jet origin—the boundary layer approximation still holds. Neglecting the pressure gradient, the governing equations for continuity and for momentum are (White, 1974)

$$\frac{\partial \overline{u}}{\partial x} + \frac{\partial \overline{v}}{\partial y} = 0 \tag{40}$$

$$\overline{u}\frac{\partial \overline{u}}{\partial x} + \overline{v}\frac{\partial \overline{u}}{\partial y} = \frac{1}{\rho}\frac{\partial \tau}{\partial y} \tag{41}$$

It is standard practice to resolve these equations by proposing a similarity solution for the velocity distribution.

$$\frac{\overline{u}}{\overline{u}_{\max}} \approx f\left(\frac{y}{b(x)}\right) \tag{42}$$

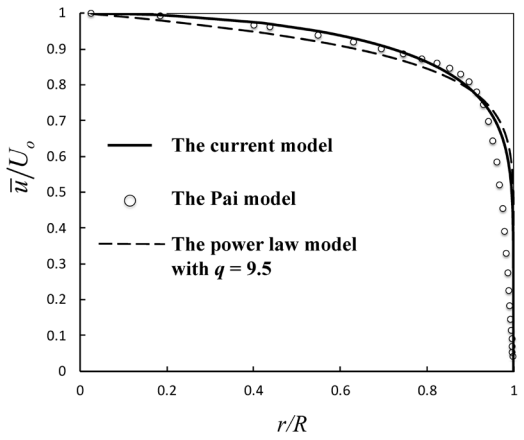

Fig. 4 Comparison among the current model (Eq. (31)), Pai model (1953) (Eq. (39)) and $1/q$-th law (Eq. (38); $q = 9.5$) (Cengel and Cimbala, 2014)

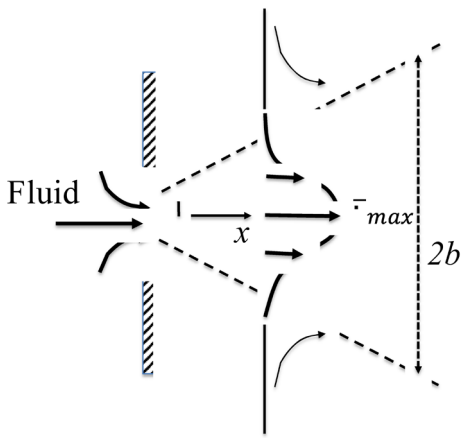

Fig. 5 Schematics of a planar jet and the velocity profile (b is the half width of the jet which is a linear function of x)

where $\bar{u}_{\max}$ denotes the maximum velocity at the jet symmetry, and b represents the width of the jet affected region (refer to Figure 5) that is a function of x.

The aperture (the jet origin) for generating the plane jet flow has a characteristic geometrical parameter, i.e., width h; the dimensionless distance from the jet origin (the orifice or the nozzle) has been noted as x/h. The analytical solution could not be obtained unless an eddy viscosity was assumed. The common procedure is employing the mixing length theory of Prandtl, which incurs eddy viscosity conforming to

$$\mu_t \approx K\rho\bar{u}_{\max} b(x) \tag{43}$$

where K represents a dimensionless constant and $\bar{u}_{\max}$ is dependent on x. If it is not $\sim 1/b$, μ_t is not constant. Through the momentum theorem and the requirement for achieving similarity for a planar jet, we get

$$\bar{u}_{\max} = \sqrt[2]{\frac{C_o}{\rho b(x)}} \tag{44}$$

$$b(x) = C_1 x \tag{45}$$

where C_o [kg·s^{-1}] and C_1 (dimensionless) are constants. As such, Eq. (43) states that the eddy diffusivity increases with distance from the jet origin at $x^{0.5}$. Based on the above, similarity solutions can be obtained; one of the typical solutions known to be similar to the laminar jet flow is the Cole's Law of the Wake model given as

$$\frac{\bar{u}}{\bar{u}_{\max}} \approx \cos^2\left(\frac{\pi}{4}\frac{y}{y_{0.5}}\right) \tag{46}$$

where $y_{0.5}$ is the location for any jet flow where the axial velocity is reduced to half of the centerline velocity. This model overestimates the experimental data from $y_{0.5}$ to the center line for the location far downstream or far field (White, 1974). Further, it is said that $y_{0.5}$ is 1/2 of $b(x)$. In the literature, the Gaussian distribution function is quoted as being able to describe the same axial velocity profile with a "tail" extending "into" the bulk fluid

$$\frac{\bar{u}}{\bar{u}_{\max}} \approx \exp\left(-\left(\frac{y}{y_c}\right)^2\right) \tag{47}$$

where y_c is a characteristic distance and is said to be the 1/e-width of the profile that is a function of x. These suggest that after a distance of x/h, the axial velocity profile becomes self-similar. Scaling using $y_{0.5}$ or y_c will collapse all axial velocity profiles under turbulent flow.

Experimental studies by Namer and Otugen (1988) and Deo *et al.* (2008) are considered significant contributions to the understanding of the turbulent planar jet. In both works, the development from the jet origin to the self-similar state was shown to be gradual. Violeau (2017) provides an analytical account of the turbulent plane jet that starts off using the well-known k–ε turbulence model. The self-similarity of the velocity profiles was assumed first to allow proceeding of the derivations. It is not simple to model a turbulent planar jet despite the already wide use of RANS models. Many numerical predictions do not match well with experimental measurements (Deo, 2005).

In the current analysis, the effect of turbulence is benchmarked with the characteristics of the jet origin (i.e., the friction velocity at the wall inside the plane jet conduit or orifice duct, and a wall-layer thickness that encapsulates the kinetic viscosity of the fluid and friction velocity). The analysis conducted in this study does not assume self-similarity.

To make the situation solvable, an effective velocity is used to approximate the convection term in the momentum equation.

$$\bar{u}_e\frac{\partial\bar{u}}{\partial x} + \bar{v}_e\frac{\partial\bar{u}}{\partial y} \approx \frac{\partial}{\partial y}\left(\upsilon\frac{\partial\bar{u}}{\partial y} - \frac{\tau_t}{\rho}\right) \tag{48}$$

where τ_t denotes the turbulent shear stress (Pa).

Incorporating the continuity Eq. (40) with the above equation, one can have

$$-\bar{u}_e\frac{\partial\bar{v}}{\partial y} + \bar{v}_e\frac{\partial\bar{u}}{\partial y} \approx \frac{\partial}{\partial y}\left(\upsilon\frac{\partial\bar{u}}{\partial y} - \frac{\tau_t}{\rho}\right) \tag{49}$$

The subscript e denotes the "effective value." Integrating the above from $y=0$ to $y>0$, one has:

$$\left(\bar{v}_e\bar{u} - \overline{vu}_e\right) - \bar{v}_e\bar{u}_{\max} \approx \left(\upsilon\frac{\partial\bar{u}}{\partial y} - \frac{\tau_t}{\rho}\right) + \left(\frac{\tau_t}{\rho}\right)_{y=0} \tag{50}$$

Dividing both sides with $\bar{u}_{\max}$ and considering the following dimensionless velocities,

$$\phi = \frac{\bar{u}}{\bar{u}_{\max}}, \quad \xi = \frac{\bar{v}}{\bar{u}_{\max}} \tag{51}$$

we get

$$-\phi_e\xi + \xi_e(\phi - 1) \approx \left(\frac{\upsilon}{\bar{u}_{\max}}\frac{\partial\frac{\bar{u}}{\bar{u}_{\max}}}{\partial y} + \frac{\overline{u'v'}}{\bar{u}_{\max}^2}\right) - \frac{(\overline{u'v'})_{y=0}}{\bar{u}_{\max}^2} \tag{52}$$

This simplifies the task of demonstrating the effect of turbulence without involving great complicity.

The Reynolds stress can be expressed as Eq. (15) with $p=m=2$ and $n=8$. When a pseudo-equilibrium state for the Reynolds stress is considered, Eq. (16) can be used. In the theoretical analysis of the turbulent planar jet given by Violeau (2017), a few assumptions were considered, including the production-to-dissipation equilibrium for turbulent quantities. Upon taking a closer look at the model by Violeau (2017), it has the same merit as that argued in Eq. (17).

Equation (52) can be further written as

$$-\phi_e\xi + \xi_e(\phi - 1) \approx \left(\frac{\upsilon}{\bar{u}_{\max}}\frac{\partial\phi}{\partial y} + \frac{\upsilon}{\bar{u}_{\max}}\left(\frac{k_g}{k_d}\right)^{\frac{1}{2}}\bar{u}^6\frac{\partial\phi}{\partial y}\right) - \frac{(\overline{u'v'})_{y=0}}{\bar{u}_{\max}^2} \tag{53}$$

Unlike previous works that used the half-width of the jet (or half of that) to scale the problem, the property of the jet origin is used as in Eq. (6).

$$\delta_v = \frac{v}{u_r} \tag{6}$$

Considering the dimensionless distance from the center line at $y = 0$,

$$\eta = \frac{y}{\delta_v} \tag{54}$$

From Eq. (53), the following:

$$-\phi_e \xi + \xi_e(\phi - 1) \approx \left(\frac{u_r}{\overline{u}_{\max}} \frac{\partial \phi}{\partial \eta} + \frac{u_r}{\overline{u}_{\max}} \frac{1}{7} \left(\frac{k_g}{k_d} \right)^{\frac{1}{2}} u_r^6 \frac{\overline{u}_{\max}^6}{u_r^6} \frac{\partial \phi^7}{\partial \eta} \right) - \frac{(\overline{u'v'})_{y=0}}{\overline{u}_{\max}^2} \tag{55}$$

The last term on the RHS by comparison with the centerline velocity squared is considered a small value and is hence neglected. Defining the following ratios,

$$\xi_e = \frac{\overline{v}_e}{\overline{u}_{\max}} \tag{56}$$

$$\varphi = \frac{\overline{u}_{\max}}{u_r} \tag{57}$$

$$\omega = \frac{1}{7} \left(\frac{k_g}{k_d} \right)^{\frac{1}{2}} u_r^6 \tag{58}$$

Further, after some manipulations,

$$-\phi_e \xi + \xi_e(\phi - 1) \approx \left(\frac{1}{\varphi} + 7\omega \varphi^5 \phi^6 \right) \frac{\partial \phi}{\partial \eta} \tag{59}$$

Equation (59) explicitly shows the separate contributions from the laminar and turbulent effects. The higher order power dependence of the velocity has a higher effect as φ increases. One further simplification is to consider ξ to be an average value, which makes the solution lose the curvature details; however, it does not affect the "bulk" prediction of the velocity profile.

$$-\phi_e \xi_e + \xi_e(\phi - 1) \approx \left(\frac{1}{\varphi} + 7\omega \varphi^5 \phi^6 \right) \frac{\partial \phi}{\partial \eta} \tag{60}$$

A numerical integration of Eq. (60) with the following estimates and a step size of 0.1 (similar result can be obtained with 0.05) can yield "bulk" velocity profiles at different ratios for φ. The following numerical values were obtained.

$$\xi_e = \frac{\overline{v}_e}{\overline{u}_{\max}} \approx \frac{1}{20} = 0.05 \quad \text{(Cushman-Roisin, 1974)}$$

$$\phi_e = \frac{\overline{u}_e}{\overline{u}_{\max}} = 0.5 \quad \text{(a good guess no doubt)}$$

$$\omega = \frac{1}{7} \left(\frac{k_g}{k_d} \right)^{\frac{1}{2}} u_r^6 = 2.31 \times 10^{-7}$$

$(= \alpha$ already obtained in the pipe flow section)

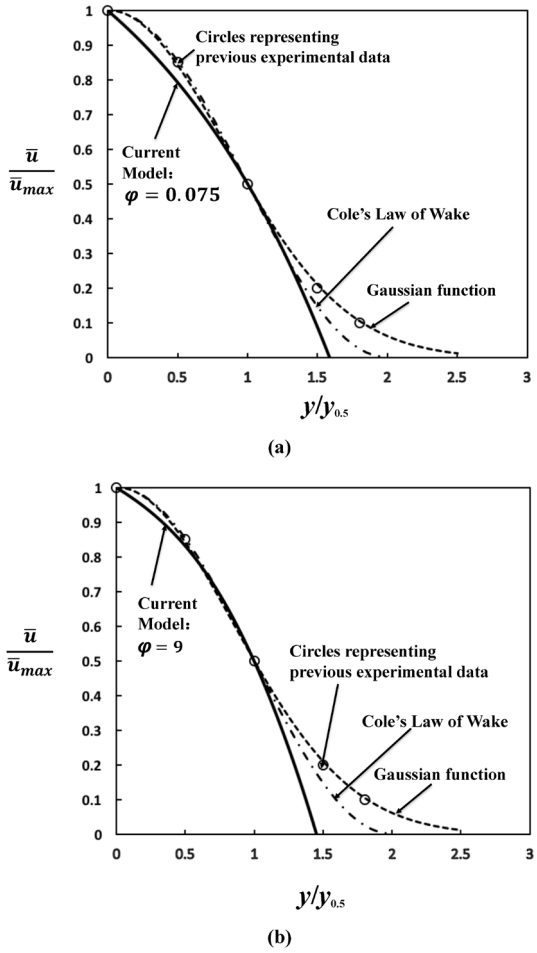

Fig. 6 Comparison among the models and experimental data (represented by a few circles indicative of the majority of data points compiled in White (1974). (a) when φ is 0.075 which is a situation that the turbulence effect (2nd term on the RHS) is small (towards the laminar scenario); (b) when φ is 9 where the turbulence effect is obvious. Here $y_{0.5} = 1$. The Gaussian function is tuned to give half of the velocity at $y_{0.5} = 1$, thus $\bar{u}/\bar{u}_{\max} \approx \exp(-0.693(y/y_{0.5})^2)$

The most important turbulence parameter $\omega = \alpha$ is inherited from the analyses from the ULW.

The above yielded a good prediction of the bulk behavior of the time-averaged axial velocity profile when benchmarked against both Cole's (Eq. (46)) and Gaussian models (Eq. (47)). Exceptions are found only at the two ends (especially at the low end of the velocity) of the profile (**Figure 6**).

Previous analytical works on turbulent plane jets focused on producing dimensionless plots such as that shown in Figure 6, and they had to pre-claim self-similarity. The effect of turbulence was not demonstrated explicitly (White, 1974; Mossad and Deo, 2015; Violeau, 2017). Using Eq. (60), the turbulence effect is explicitly shown with the parameter φ. The greater the φ, the greater is the influence of turbulence on the overall flow.

In terms of the turbulence in an internal flow such as pipe flow, the friction velocity is approximately 5 to 20%, which is

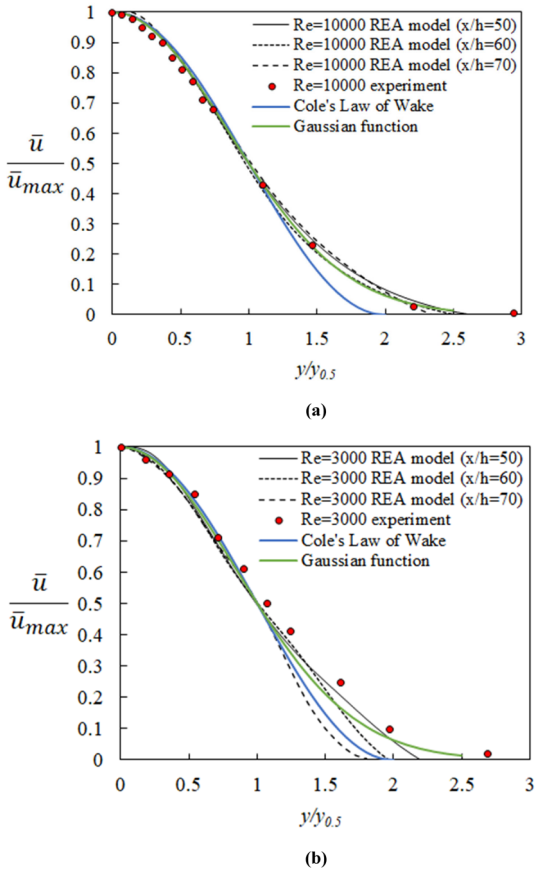

Fig. 7 Simulation results for (a) $Re = 10{,}000$ and (b) $Re = 3{,}000$ (the far-field results are shown to match experimental data and from the classic analyses)

typically the mean velocity (Schlichting and Gersten, 2003). In other words, the mean velocity is 5–20 times the friction velocity. φ should then range from 5 to greater than 20.

Based on Eqs. (44), (45) and according to White (1974), we get

$$x = \frac{C_o}{C_1}\frac{\bar{u}_{max}^2}{\rho} \tag{61}$$

or,

$$\left(\frac{x_2}{x_1}\right)^{0.5} = \frac{\bar{u}_{max,1}}{\bar{u}_{max,2}} \tag{62}$$

where $x_2 > x_1$ and $\bar{u}_{max,2} < \bar{u}_{max,1}$. Considering $x_1 = 5h$, which is very close to the jet origin, h denotes the slot height if the plane jet is placed horizontally such as that in the work by Deo (2005), and one can see that only after a distance of $20h$, the maximum velocity (the time-averaged axial velocity at $y = 0$) is reduced to half. To demonstrate a practical scenario, Deo (2005) used a slot size of $h = 5.6$ mm. For example, at $x = 5h$ from the jet origin or in the proximity of the jet origin, φ is 9. After another $15h$, it would drop to 4.5, which is within the range where the dimensionless time-averaged axial velocity can be scaled by $y_{0.5}$, thereby yielding a self-similar velocity profile.

Based on the above analyses, further interesting works can be performed based on the definition and derivations of γ for higher dimensions. Indeed, the ULW is not absolutely universal, especially in the log-law region and beyond, and it depends on the pressure gradient, compressibility, and even Re numbers (Barenblatt *et al.*, 1997; Trinh, 2010; Liu and Wu, 2017; Luchini, 2017). These effects are not addressed here.

1.3.2 Numerical solutions As mentioned above, it is not possible to obtain an analytical solution in the current study to demonstrate the matching of the full range of velocity profiles. To demonstrate the current approach, a more elaborate numerical simulation was considered. The model has been laid out in the framework of solving fluid equations using FLUENT (see Appendix 2). **Figure 7** shows that the results of dimensionless velocity profiles are in good agreement with the available experimental data for the far field. This suggests that the REA model has good potential for more extensive studies in the future.

Conclusion

A new idea was proposed for formulating or constructing a Reynolds stress equation. Coupling with momentum balance, the conformity of the model to the ULW was demonstrated. Reynolds stress generation and dissipation were both considered in a nonconventional approach, which is REA-T because of the emphasis of molecular-level interaction and the employment of power-law-like rate equations. The local turbulence, as soon as it is generated, begins to dissipate at the same location. The same model structure is found to describe the velocity profile for fully developed turbulent flow in a circular pipe. The solution reduces naturally to the laminar parabolic profile as *Re* decreases.

The approach was then extended to describe the turbulent planar jet. The prediction of the bulk velocity profile was found to be reasonable. A fuller model with diffusive and convective transport was designed using the same Reynolds stress function to simulate the jet flow. This shows that the far-field dimensionless velocity profiles match the historical data. It is hoped that the initial work described here will be useful for the future explorations of REA-T for engineering purposes.

Acknowledgement

The first author XDC likes to dedicate this study to his late father, Prof. Naixing Chen (1933–2018), who was a leading academic and engineer in the field of flow in turbine machines internationally; he was the first to lead XDC into the field of fluid mechanics just over thirty seven years ago. The second author, SYZ, has contributed to the numerical simulations of the planar jet flow. Discussions sought from Professor Yu Zhang at Tsinghua University, Associate Professor Meng Wai Woo at the University of Auckland, and Professor Jie Xiao at Soochow University are gratefully acknowledged.

Literature Cited

Avila, K., D. Moxey, A. de Lozar, M. Avila, D. Barkley and B. Hof; "The

Onset of Turbulence in Pipe Flow," *Science*, **333**, 192–196 (2011)
Barenblatt, G. I., A. J. Chorin and V. M. Prostokishin; "Scaling Laws for Fully Developed Turbulent Flow in Pipes: Discussion of Experimental Data," *Proc. Natl. Acad. Sci. U.S.A.*, **94**, 773–776 (1997)
Barkley, D., B. Song, V. Mukund, G. Lemoult, M. Avila and B. Hof; "The Rise of Fully Turbulent Flow," *Nature*, **526**, 550–553 (2015)
Bird, R. B., W. E. Stewart and E. N. Lightfoot; Transport Phenomena, 2nd ed., pp. 152–168, John Wiley and Sons, New York, U.S.A. (2002)
Cengel, Y. A. and J. M. Cimbala; Fluid Mechanics: Fundamentals and Applications, 3rd ed., pp. 322–343, McGraw-Hill, New York, U.S.A. (2014)
Chen, C. J.; Fluid Mechanics and Heat Transfer–Laminar, Turbulent and Computational (English Monograph Translated by East China Institute of Engineering, Nanjing), p. 385, Defense Industry Press, China (1984)
Chen, X. D.; "Laminar to Turbulence Transition Revealed through a Reynolds Number Equivalence," *Engineering*, **5**, 576–579 (2019)
Churchill, S. W.; "New Simplified Models and Formulations for Turbulent Flow and Convection," *AIChE J.*, **43**, 1125–1140 (1997)
Churchill, S. W.; "Progress in the Thermal Sciences: AIChE Institute Lecture," *AIChE J.*, **46**, 1704–1722 (2000)
Cushman-Roisin, B.; Environmental Fluid Mechanics, Chapter 9, John Wiley and Sons, New York, U.S.A. (1974)
Deo, R. C.; "Experimental Investigation of the Influence of Reynolds Number and Boundary Conditions on a Plane Air Jet," Ph.D. Thesis, the University of Adelaide, Adelaide, South Australia (2005)
Deo, R. C., J. C. Mi and G. J. Nathan; "The Influence of Reynolds Number on a Plane Jet," *Phys. Fluids*, **20**, 075108 (2008)
Eskin, D.; "Modeling an Effect of Pipe Diameter on Turbulent Drag Reduction," *Chem. Eng. Sci.*, **162**, 66–68 (2017)
Esteban, L. B., J. S. Shrimpton and B. Ganapathisubramani; "Laboratory Experiments on the Temporal Decay of Homogeneous Anisotropic Turbulence," *J. Fluid Mech.*, **862**, 99–127 (2019)
Flint, L. F.; "On the Velocity Profile for Turbulent Flow in a Straight Pipe," *Chem. Eng. Sci.*, **22**, 1127–1131 (1967)
Hof, B., A. de Lozar, M. Avila, X. Tu and T. M. Schneider; "Eliminating Turbulence in Spatially Intermittent Flows," *Science*, **327**, 1491–1494 (2010)
Hrenya, C. M., E. J. Bolio, D. Chakrabarti and J. L. Sinclair; "Comparison of Low Reynolds Number k–ε Turbulence Models in Predicting Fully Developed Pipe Flow," *Chem. Eng. Sci.*, **50**, 1923–1941 (1995)
Kudela, H.; "Lecture Notes on Turbulent Flow," Faculty of Mechanics and Energy, Politechnika Wroclawska (Wroclaw University of Science and Technology), Poland(www.itcmp.pwr.wroc.pl/~znmp/...FM/Lecture_no3_Turbulent_flow_Modelling.pdf and https://www.coursehero.com/file/21277195/Lecture13/) (2014)
Kühnen, J., B. Song, D. Scarselli, N. B. Budanur, M. Ried, A. P. Willis, M. Avila and B. Hof; "Destabilizing Turbulence in Pipe Flow," *Nat. Phys.*, **14**, 386–390 (2018)
Laufer, J.; The Structure of Turbulence in Fully Developed Pipe Flow, National Bureau of Standards; (Report 1174), U.S.A. (1952)
Levenspiel, O.; Chemical Reaction Engineering, 3rd ed., pp. 14–26, John Wiley and Sons, New York, U.S.A. (1999)
Liu, J. and S. P. Wu; "Generalized Wall Function and Its Application to Compressible Turbulent Boundary Layer over a Flat Plate," *J. Phys. Conf. Ser.*, **822**, 012017 (2017)
Luchini, P.; "Universality of the Turbulent Velocity Profile," *Phys. Rev. Lett.*, **118**, 224501 (2017)
Mossad, R. and R. C. Deo; "Numerical Modelling of the Velocity Field of a Plane Jet Flow at Moderate Jet Reynolds Numbers," Proceedings of the 11th International Conference on CFD in the Minerals and Process Industries (CSIRO), p. 6, Melbourne, Australia (2015)
Namer, I. and M. V. Otugen; "Velocity Measurements in a Plane Turbulent Air Jet at Moderate Reynolds Numbers," *Exp. Fluids*, **6**, 387–399 (1988)
Pai, S. I.; "On Turbulent Flow in Circular Pipe," *J. Franklin Inst.*, **256**, 337–352 (1953)
Patel, V. C.; "A Unified View of the Law of the Wall Using Mixing-Length Theory," *Aeronaut. Q.*, **24**, 55–70 (1973)
Pavlíček, P.; "Local Reynolds Number," *AIP Conf. Proc.*, **2118**, 030035 (2019)
Schaefer, P., M. Gampert, J. H. Goebbert, M. Gauding and N. Peters; "Asymptotic Analysis of Homogeneous Isotropic Decaying Turbulence with Unknown Initial Conditions," *J. Turbul.*, **12**, N30 (2011)
Schlichting, H. and K. Gersten; Boundary Layer Theory, 8th ed., Springer, Berlin, Germany (2003)
Sherwood, T. K., K. A. Smith and P. E. Fowles; "The Velocity and Eddy Viscosity Distribution in the Wall Region of Turbulent Pipe Flow," *Chem. Eng. Sci.*, **23**, 1225–1236 (1968)
Spalding, D. B.; "A Single Formula for the 'Law of the Wall'," *J. Appl. Mech.*, **28**, 455–458 (1961)
Tao, J., S. Chen and W. Su; "Local Reynolds Number and Thresholds of Transition in Shear Flows," *Sci. China Phys. Mech. Astron.*, **56**, 263–269 (2013)
Thomas, F. O. and V. W. Goldschmidt; "Structural Characteristics of a Developing Turbulent Planar Jet," *J. Fluid Mech.*, **163**, 227–256 (1986)
Thornber, B., A. Mosedale and D. Drikakis; "On the Implicit Large Scale Eddy Simulations of Homogeneous Decaying Turbulence," *J. Comput. Phys.*, **226**, 1902–1929 (2007)
Trinh, K. T.; "A Zonal Similarity Analysis of Velocity Profiles in Wall-bounded Turbulent Shear Flows," arXiv:1001.1594 [physics.flu-dyn] (2010)
Violeau, D.; "A Comprehensive Presentation of the Turbulent Plane Jet Theory with Passive Scalar," *Math. Probl. Eng.*, **2017**, 4369895 (2017)
White, F. M.; Viscous Fluid Flow, pp. 434–476, McGraw-Hill, New York, U.S.A. (1974)

Appendix 1 Structuring the dissipation term for Reynolds stress

Consider the case of uniform flow (with velocity U_o) passing through a metal mesh, which is defined in the x-direction where the turbulence is introduced with the mesh and then the flow gradually settles back to laminar (Chen, 1984).

Chen (1984) explained in detail how one obtains the model constants for the k–ε and extended models. One of the experiments needed was the turbulence decay measurement in an one dimensional scenario, i.e. the flow behind a mesh. Along the x-direction, the flow is uniform with $u = U_o$ ($= 1.286\,\mathrm{m \cdot s^{-1}}$) and in the y- and z-directions, respectively, $v = w = 0$. The measurement of the turbulent kinetic energy k yields

$$k = Ax^{-1.08} \tag{A1}$$

where A denotes a constant. In this case, the relevant turbulence kinetic energy equation is

$$U_o \frac{\partial \overline{u'u'}}{\partial x} = -\overline{\dot{D}}_{uu} \tag{A2}$$

where x denotes the direction of the flow. The subscript "uu" represents the dissipation of this turbulent energy corresponding to the Reynolds stress in Eq. (A2). By definition, one has

$$k = \frac{3}{2}\overline{u'u'} \tag{A3}$$

Taking the dissipation as a power law (with power of $s>0$) based on the interaction assumption at the molecular level,

$$\frac{2}{3}U_o \frac{dk}{dx} = -k_d \left(\frac{2}{3}\right)^s k^s \tag{A4}$$

From Eq. (A1), one has

$$(-1.08)x^{-2.08} = -k_d \left(\frac{2}{3}\right)^{s-1} \frac{1}{U_o} A^{s-1} x^{-1.08s} \tag{A5}$$

Thus, one can obtain

$$s = \frac{-2.08}{-1.08} = 1.92 \tag{A6}$$

where s is rounded to 2 in this study. Decaying kinetics as that in (A1) may take somewhat different values (often within 1–1.5) in the literature (Schaefer *et al.*, 2011; Esteban *et al.*, 2019). The detailed fundamentals are not dealt with in the current work.

More generically, one can propose

$$\overline{\dot{D}_{uu}} = k_d \left(\overline{u'u'}\right)^2 \tag{A7}$$

Further generalization of this approach to all cases of $i=j$ yields

$$\overline{\dot{D}_{ii}} = k_{d,ii} \left(\overline{u_i' u_i'}\right)^2 \tag{A8}$$

Further, extending that to $i \neq j$, one has

$$\overline{\dot{D}_{ij}} = k_{d,ij} \left(\overline{u_i' u_j'}\right)^2 \tag{A9}$$

Appendix 2 Numerical simulations of the turbulent planar jet problem using the REA approach for turbulence

In numerical simulations, governing equations are similar to the turbulence boundary layer equations. Similarly, only one Reynolds stress was considered, and it was correlated to turbulence viscosity (μ_t) based on the Boussinesq hypothesis. In the pseudo-steady state, the turbulence model in the current work can be converted to the form of turbulent viscosity. Hence, the model in the pseudo-steady state is implemented as the source term in the momentum equation of the x direction. The modified momentum equations for incompressible fluid flow are given as

$$\frac{\partial \bar{u}}{\partial x} + \frac{\partial \bar{v}}{\partial y} = 0 \tag{A10}$$

$$\rho\left(\frac{\partial \bar{u}}{\partial t} + \bar{u}\frac{\partial \bar{u}}{\partial x} + \bar{v}\frac{\partial \bar{u}}{\partial y}\right) = -\frac{\partial \bar{p}}{\partial x} + \mu\left(\frac{\partial^2 \bar{u}}{\partial x^2} + \frac{\partial^2 \bar{u}}{\partial y^2}\right) + \frac{\partial\left(-\rho\overline{u'v'}\right)}{\partial y} \tag{A11}$$

$$\rho\left(\frac{\partial \bar{v}}{\partial t} + \bar{u}\frac{\partial \bar{v}}{\partial x} + \bar{v}\frac{\partial \bar{v}}{\partial y}\right) = -\frac{\partial \bar{p}}{\partial y} + \mu\left(\frac{\partial^2 \bar{v}}{\partial x^2} + \frac{\partial^2 \bar{v}}{\partial y^2}\right) \tag{A12}$$

$$\frac{\partial\left(-\rho\overline{u'v'}\right)}{\partial y} = \frac{\partial}{\partial y}\left(\mu_t \frac{\partial \bar{u}}{\partial y}\right) \tag{A13}$$

$$\mu_t = \mu\left(\frac{k_g}{k_d}\right)^{1/2} \bar{u}^6 \tag{A14}$$

where $\bar{u}$ and $\bar{v}$ represents the mean velocity components in the x and y direction [m/s], respectively; ρ denotes the air density [kg/m^3]; μ denotes the air viscosity [kg/(m·s)]; $\bar{p}$ denotes the mean fluid pressure [Pa]; and $[k_g/k_d]^{1/2}$ in Eq. (17) can be calculated based on α, which is defined as

$$\alpha = \frac{1}{7}\left(\frac{k_g}{k_d}\right)^{\frac{1}{2}} \left(\sqrt{\frac{\tau_w}{\rho}}\right)^6 = 2.31\times10^{-7} \tag{A15}$$

where the wall shear stress τ_w can be evaluated using ULW. The simplest method is to obtain it using the friction factor in turbulence pipe flow.

$$\tau_w = \frac{f\rho u^2}{8} \tag{A16}$$

$$f \approx 0.316\, Re^{-1/4} \tag{A17}$$

where $Re = \rho u d/\mu$ is the Reynolds number in the pipe flow, and length d is equal to the height of the nozzle exit of the jet flow. The computational domain and typical mesh distribution are shown in **Figure A1**. The size of the nozzle, air properties, and experimental data were derived from the literature provided by Deo *et al.* (2008).

A structured mesh was generated for the entire computational domain.

The boundary conditions applied in the simulations are summarized as follows. The nozzle exit was set as the velocity inlet in the simulation. The velocity distribution at the nozzle exit was specified by the hyperbolic tangent profile provided by Thomas and Goldschmidt (1986).

$$u = \frac{u_{\text{avg}}}{2} + \frac{u_{\text{avg}}}{2}\tanh\left(\frac{-|y - y_c| + 0.5h}{2\theta}\right) \tag{A18}$$

$$v = 0 \tag{A19}$$

where u_{avg} denotes the mean velocity of the nozzle exit (m/s), which can be approximatively calculated based on the exit Reynolds number; y and y_c denote the y coordinate values of the inlet and the inlet midpoint, respectively (m); h represents the height of the nozzle exit (m); and θ denotes the shear layer momentum thickness (m), which was already

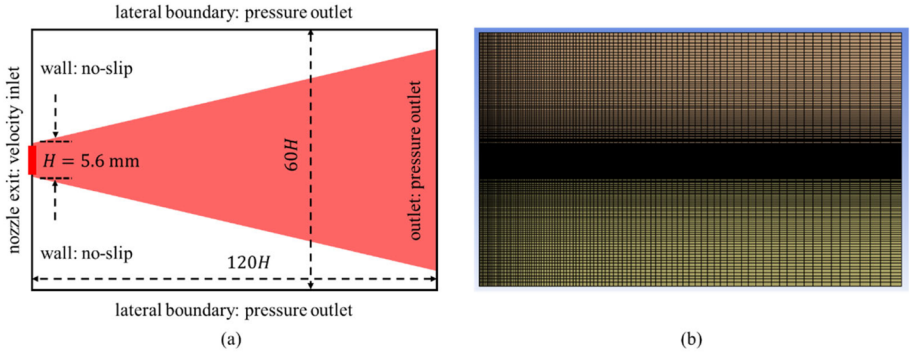

Fig. A1 Schematic showing: (a) the computational domain and boundary conditions, the red shadow shows the typical spread region of jet; (b) the mesh, finer mesh can be observed at the region near the nozzle exit and the center of jet

measured in the experiment conducted by Deo *et al.* (2008).

The outlet and lateral boundary are the pressure outlet, applying a fixed value (the gauge pressure is 0) for pressure and zero gradients for velocity. The wall adjoining the nozzle exit was considered as the no-slip boundary. The pressure and velocity are initialized as 0 to represent the quiet ambient air at the initial time. The governing equations are solved in ANSYS Fluent in the transient state. The semi-implicit method for pressure-linked equations (SIMPLE) was employed for pressure velocity coupling. The gradient scheme is least squares cell-based. The second-order upwind scheme was chosen for the spatial discrete of the momentum equation. The pressure staggering option (PRESTO) scheme was applied for pressure. All discretized algebraic equation systems were solved using an iterative solver until the residual values were less than the convergence criterion, which were set as 1×10^{-3} for all equations. The time step is set based on the Courant–Friedrichs–Lewy (CFL) condition to ensure that the CFL number is less than 1. The time-averaged process is continually performed in the computation process until the mean velocity reaches a steady condition, the computation is then terminated, and the data are saved for further analysis. The half-width, centerline velocity, and lateral velocity can be calculated based on the final velocity field.